Synchronous Reluctance Machine with Controlled Capacitance Injection

A.S.O Ogunjuyigbe[1], A.A Jimoh[1], *member IEEE*, D.V Nicolae[1], *member IEEE and* J.T Agee[2]

[1] Department of Electrical and Electronic Engineering
Tshwane University of Technology,
P.O.Box X680, Pretoria 0001. South Africa

[2] Department of Electrical Engineering
University of Botswana,
Botswana.

Email: Jimohaa@tut.ac.za, aogunjuyigbe@yahoo.com , danaurel@yebo.co.za, agee@mopipi.ub.bw

***Abstract*— This paper describes a detailed analysis, verified by practical experimental results, of a synchronous reluctance machine with two similar stator windings and capacitance injection using a static switch. The steady state equivalent circuit is developed and used to investigate leading capacitance injection into the machine via a balanced three phase auxiliary winding that is only magnetically coupled to the main winding. The scheme was found to improve the torque and power factor performance of the machine as well as reduce harmonics in the line current. Two switching topologies were utilized for the static control in this arrangement, and both were found to present good and comparable results. Experimental results corroborate the simulations.**

I. INTRODUCTION

Synchronous reluctance machines (syncrel) are rugged, simple in structure, and cheaper to manufacture as compared with other types of AC machines. It has attracted intensive research efforts for several decades to improve its performance characteristics. These research efforts were mostly focused on the rotor design of the machine, and it has led to the emergence of the following rotor configurations: 1) Simple salient structure, 2) Segmented rotor type, 3) Flux barrier type, 4) Transversely laminated and 5) Axially laminated type.

The machine makes use of a standard three phase stator of an induction machine and any of the rotor configurations listed above.

The performance of Syncrel has been identified in literatures [1 -7] to be dependent on the ratio of the d-axis inductance to the q-axis inductance (L_d/L_q) and their difference (L_d-L_q).

Syncrel has also been shown to provide attractive torque per ampere, and power factor when vector controlled. Furthermore, the advantages offered by multi-phase machine have been explored. A five phase synchronous reluctance machine has been studied and controlled to utilize the third harmonic component of the current for torque improvement. A 10% torque improvement was reported [6, 7].

The power factor of a synchronous reluctance can be improved by reactive power compensation through the installation of capacitor banks; however these capacitor banks have been found to result in problems particularly when there is a loss of supply. If the capacitors are series connected and external, it will invariably lower the overall impedance of the machine and result in higher output power. Conversely, the achieved output power will be obtained at a cost of larger currents and a negligible improvement in power factor. Also, using a shunt capacitor on the other hand improves the power factor of the external supply rather than the inherent power factor of the machine [1]. It was likewise reported in [8] that the use of either of these methods can cause problems at light load conditions and relatively expensive switchgear are required to vary the capacitance value with load changes. Thus the use of either the external series or the shunt capacitor seems not to present a practical method for the improvement of the power factor.

This paper then aims at discussing an approach that improves performance of a synchronous reluctance machine by the use of an additional winding identified as auxiliary winding in the stator. The auxiliary winding is connected to a capacitor bank through a static converter. The conceptual diagram is as shown if Fig.1.

II. ELECTRICAL EQUIVALENT CIRCUIT

A. Machine Structure

The conceptual diagram of the machine structure discussed in this paper is as shown in figure 1. The main winding 'abc' is connected to the mains supply while the auxiliary winding 'xyz' is connected to a static switch that is utilized to inject a leading reactive power into the machine for power factor improvement. The two windings (main and auxiliary) are magnetically coupled, have the same number of poles and are sinusoidally distributed.

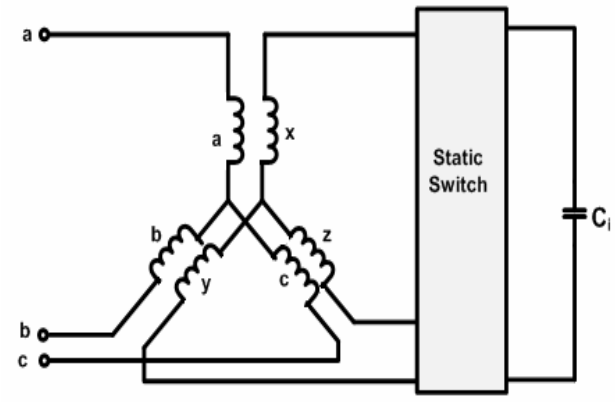

Fig. 1: Stator Winding arrangement with the Static Switch.

B. Machine Mathematical Model

The electrical voltage equations that describe the behavior of the machine structure are written in matrix form as:

$$V_{abc} = R_s I_{abc} + \tfrac{d}{dt}\lambda_{abc} \tag{1}$$

$$V_{xyz} = R_s I_{xyz} + \tfrac{d}{dt}\lambda_{xyz} \tag{2}$$

where:

$$\lambda_{abc} = L_{abc} I_{abc} + L_{abcxyz} I_{xyz} \tag{3}$$

$$\lambda_{xyz} = L_{xyzc} I_{xyz} + L_{xyzabc} I_{abc} \tag{4}$$

gives the flux linkages of the windings.

L_{abc} and L_{xyz} represent the self and mutual inductances of each of the stator winding, while L_{abcxyz} and L_{xyzabc} represent the mutual inductances between the two windings.

where :

$$L_{abc} = \begin{bmatrix} L_{aa} & L_{ab} & L_{ac} \\ L_{ba} & L_{bb} & L_{bc} \\ L_{ca} & L_{cb} & L_{cc} \end{bmatrix} \tag{5}$$

$$L_{xyz} = \begin{bmatrix} L_{xx} & L_{xy} & L_{xz} \\ L_{yx} & L_{yy} & L_{yz} \\ L_{zx} & L_{zy} & L_{zz} \end{bmatrix} \tag{6}$$

$$L_{abcxyz} = L^{T}_{xyzabc} = \begin{bmatrix} L_{ax} & L_{ay} & L_{az} \\ L_{bx} & L_{by} & L_{bz} \\ L_{cx} & L_{cy} & L_{cz} \end{bmatrix} \tag{7}$$

The self and mutual inductances in equations (5)-(7) are evaluated using the method of winding function theory and is expressed as:

$$L_{ij} = (\mu_o \times r \times l)\int g^{-1}(\phi,\theta_{rm}) N_i(\phi,\theta_{rm}) N_j(\phi,\theta_{rm}) d\phi \tag{8}$$

where *r* is the inner radius of the stator, *l* is the effective magnetic length of the machine and *Ni,j* is the winding distribution of the two stator windings.

The inductance components of equations (5)-(7) obtained using (8) are time varying, consequently , the voltage equations of (1) and (2) are time varying and this will actually be complicated to resolve. The d-q transformation is then used, thus multiplying equations (1) and (2) by the appropriate transformation matrix (T (θ)), we can write

$$T(\theta)V_{abc} = R_s T(\theta) I_{abc} + T(\theta)\frac{d\lambda_{abc}}{dt} \tag{9}$$

$$T(\theta)V_{xyz} = R_s T(\theta) I_{xyz} + T(\theta)\frac{d\lambda_{xyz}}{dt} \tag{10}$$

The second term of the right hand side of equations (9) and (10) can be further expanded and written as:

$$T(\theta)\frac{d\lambda_{abc}}{dt} = \frac{d}{dt}[T(\theta)\lambda_{abc}] - \frac{dT(\theta)}{dt}T(\theta)^{-1}T(\theta)\lambda_{abc} \tag{11}$$

Substituting the appropriate matrices, the second component of equation (11) expands to:

$$T(\theta)\frac{dT(\theta)^{-1}}{dt} = \omega\begin{bmatrix} 0 & 1 & 0 \\ -1 & 0 & 0 \\ 0 & 0 & 0 \end{bmatrix} = \varpi \tag{12}$$

When the stator flux linkages of equations (3) and (4) are multiplied by the appropriate transformation matrix (T (θ)), it yields the flux linkages in the d-q system as:

$$\lambda_{qd01} = L_{qd01} I_{qd01} + L_{qd012} I_{qd02} \tag{13}$$

$$\lambda_{qd02} = L_{qd021} I_{qd01} + L_{qd02} I_{qd02} \tag{14}$$

Using equations (11)-(14) in (9) and (10), it yields:

$$V_{qd01} = R_s I_{qdo1} + \frac{d\lambda_{qd01}}{dt} + \varpi\lambda_{qd01} \tag{15}$$

$$V_{qd02} = R_s I_{qdo2} + \frac{d\lambda_{qd01}}{dx} + \varpi\lambda_{qd02} \tag{16}$$

From equations (13)-(16), the equivalent circuit of the machine can be drawn as in Fig. 2.

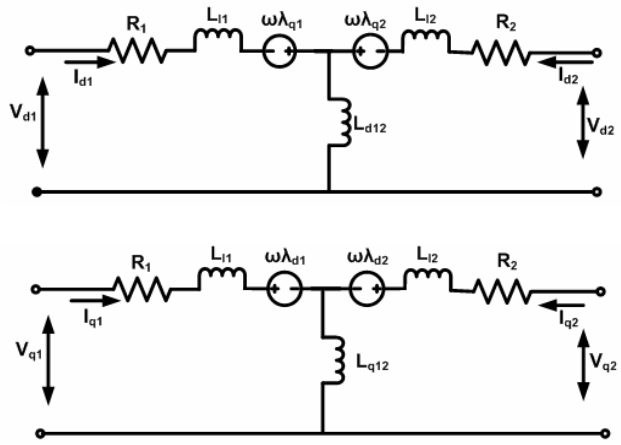

Fig. 2: DQ equivalent circuit of the machine

C. Per Phase Equivalent circuit

The complex form of equations (13)-(16) can be expressed as:

$$V_{qd01} = R_s I_{qdo1} + \frac{d\lambda_{qd01}}{dt} + j\varpi\lambda_{qd01} \tag{17}$$

$$V_{qd02} = R_s I_{qdo2} + \frac{d\lambda_{qd01}}{dx} + j\varpi\lambda_{qd02} \tag{18}$$

and

$$\lambda_{qd01} = L_1 I_{qd01} + L_m I_{qd02} \tag{19}$$

$$\lambda_{qd02} = L_m I_{qd01} + L_2 I_{qd02} \tag{20}$$

Under the steady state condition, the state derivatives of equations (17), (18) are set to zero; thus substituting (19), (20) into (17), (18), the resulting steady state equation is given by:

$$V_{qd01} = R_1 I_{qdo1} + j\omega(L_1 - L_m) I_{qdo1} + j\omega L_m (I_{qdo1} + I_{qdo2}) \quad (21)$$

$$V_{qd02} = R_2 I_{qdo2} + j\omega(L_2 - L_m) I_{qdo2} + j\omega L_m (I_{qdo1} + I_{qdo2}) \quad (22)$$

Applying appropriate inverse transformations to equations (22) and (23), the per phase equivalent equations of the machine can be written as:

$$V_a = R_1 I_a + j\omega L_{l1} I_a + j\omega L_m (I_a + I_x) \quad (23)$$

$$V_x = R_2 I_x + j\omega L_{l1} I_x + j\omega L_m (I_a + I_x) \quad (24)$$

From which we can draw the per phase equivalent circuit of the machine as

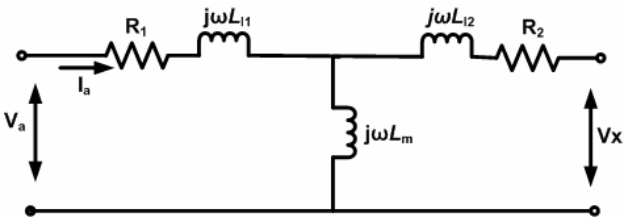

Fig. 3: Per phase steady state Equivalent circuit

Bearing in mind that the auxiliary winding 'xyz' is attached to a static switch that is used for appropriate capacitance injection for power factor improvement, the per phase equivalent circuit is then redrawn to include static switch as shown in Fig. 4.

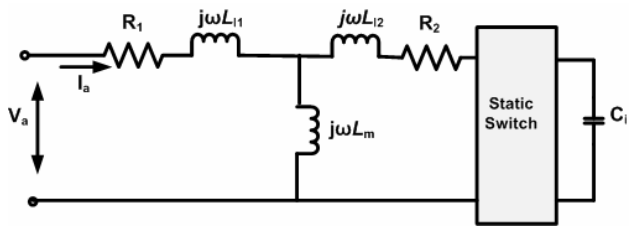

Fig. 4: Per Phase Equivalent circuit with the Static switch

III. Static Switches And Their Control

The static switch as shown in Fig. 4 can be used to provide an equivalent capacitive reactance for reactive power compensation of the machine at different load angles.

In this paper, two topologies of static switches have been studied. The per phase circuit of the first one is shown in Fig. 5. It is a simple "double switch" topology (DST) that makes use of a few numbers of bilateral switches (two).

The main capacitor C_1 is introduced into the auxiliary winding circuit via a bidirectional switch Sw_1 for a period of time depending on the duty cycle (D) of the switching frequency. During this time the bidirectional switch Sw_2 is OFF.

When Sw_1 is OFF, the capacitor is discharged. The discharging current is limited by R_d which affects the

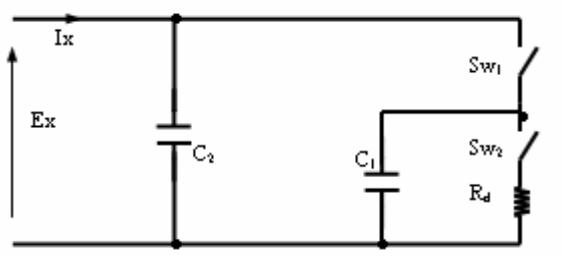

Fig. 5 Two switches topology

capacitive compensation effect. The capacitor C_2, though much smaller than C_1 is connected to mitigate the spikes during switching off the main capacitor. Thus, the equivalent capacitor can be written as:

$$C_{eq} = D \times C_1 + C_2 \quad (25)$$

The second switching topology (Bridge Switch Topology – BST)) studied is presented in Fig.6. It was proposed in [10] as a solution for compensation power factor in inductive circuits.

In this topology, the equivalent capacitance can be written as:

$$C_{eq} = C_2 + \frac{C_1}{(2D-1)^2} \quad (26)$$

Observing from (26), the size of the capacitor C_1 in this topology should be significantly reduced.

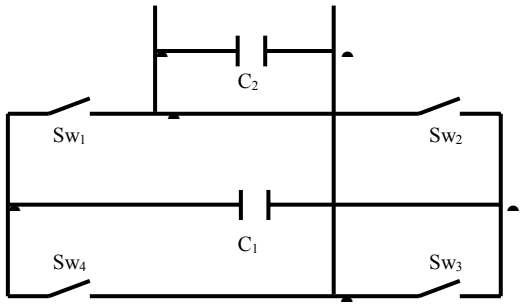

Fig. 6 Bridge switch topology

The switches used in the above topologies are IGBTs configured in the bilateral mode as shown in Fig. 7.

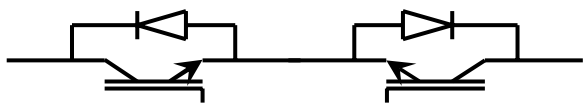

Fig. 7 Bilateral switch

IV. Simulation Results

The switching arrangements of Figs. 5 and 6 were simulated in the Matlab/Simulink environment to observe the compensational effect of the capacitance injected into the auxiliary winding on the machine performance and at different switching frequency.

In the simulation, switching frequencies of 1kHz and 5kHz were considered and reported in this work.

Fig. 8 shows the phase voltage (V_a), phase current (I_a) and the auxiliary winding current (I_x), of the unloaded machine for a duty cycle of 5% and frequency of 1 kHz; while Fig. 9 shows the same result but for a switching frequency of 5 kHz.

From these two figures it is observed that the main supply current I_a is minimally affected at a switching frequency of 5 kHz, and closely represent a sinusoid.

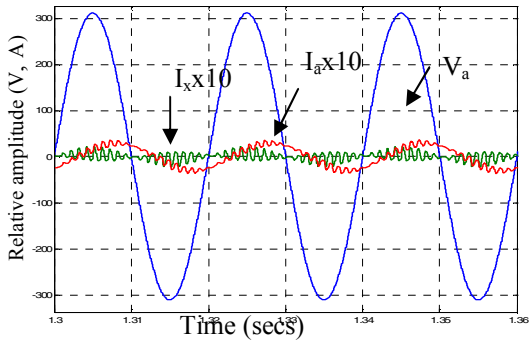

Fig.8 Steady-state parameters for f = 1 kHz duty cycle 5%

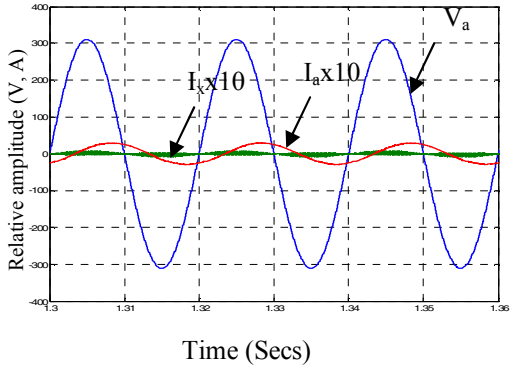

Fig.9 Steady-state parameters for, f = 5 kHz , duty cycle 5%

At this frequency of 5 kHz, using a duty cycle of 80%, the power factor of the machine was compensated to unity. The zero crossing of both phase voltage and current demonstrating this compensation are displayed in Fig. 10.

The fundamental component of the main winding current and THD for the 5 kHz frequency is displayed in the spectrum window of Fig. 11.

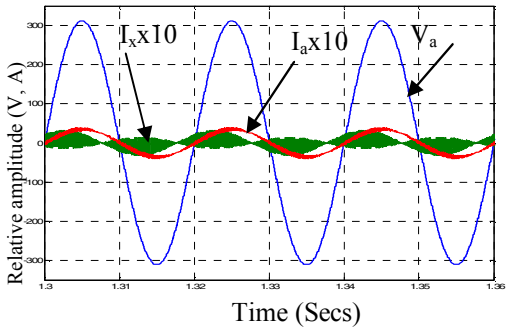

Fig.10 Steady-state parameters for, f = 5 kHz, duty cycle 80%

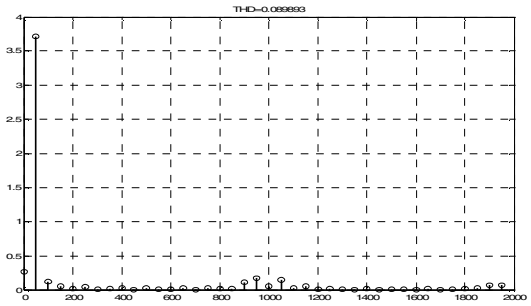

Fig.11 Harmonic distortion of the main winding current at f = 5 kHz and, duty cycle 80%

The machine was simulated with the application of full load and the results are as displayed in Figs. 12 and 13.

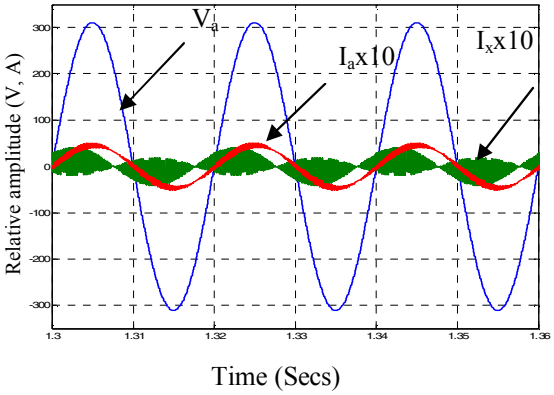

Fig.12 Steady-state parameters for f = 5 kHz, duty cycle 80% under Load Condition

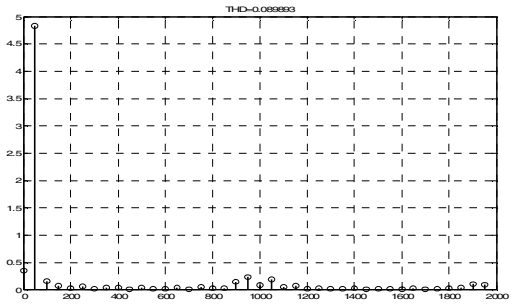

Fig.13 Harmonic distortion of the main winding current at f = 5 kHz and, duty cycle 80%

Fig.12 gives the relative amplitude of the phase voltage, current and the auxiliary current, while Fig.13 gives the spectrum of the fundamental component of the main winding current and the total harmonic distortion for a frequency of 5 kHz and under the new loading condition.

It is easily observed from these figures that the voltage and the current are in phase indicating good compensation even under the present loading condition.

The simulation using the bridge switch topology of Fig. 6 gave the same result as that of the two switch topology but at a duty cycle of 60%, and the capacitance required is smaller.

V. PERFORMANCE ANALYSIS

A. *Impact of the Proposed Scheme on Power Factor*

The use of static switches to obtain a good power factor at the main stator winding has been earlier demonstrated. This section therefore set forth the steady state characteristics of the power factor correction scheme discussed in this paper.

When the static switch is controlled to inject only leading reactive power, its effect can be represented in the equivalent circuit of Fig. 4 by a variable capacitor which is functionally dependent on the voltage across it as well as the current through it [8].With a suitable auxiliary winding, the possibility of unity power factor operation at the main winding 'abc' terminals is here demonstrated for wide range of load angles.

The total impedance of Fig. 4 when viewed from the source end can be expressed as:

$$Z_T = \left(\left(R_1 + jX_{l1} \right) + \left(X_m // (R_2 + j(X_{l2} - X_c) \right) \right) \tag{27}$$

where $X_{l1} = X_{l2} = X_1 - X_m = X_1(1-k); R_1 = R_2 = R$ and k is the coefficient of coupling between the two windings.

However, since the machine under consideration is of the salient rotor structure type, the synchronous impedance is defined as a function of the angular position of the direct axis of the rotor with respect to the axis of the mmf [1, 11]. It is expressed as:

$$X = \tfrac{1}{2}(X_d + X_q) + \tfrac{1}{2}(X_d - X_q) e^{j2\delta} \tag{28}$$

For ease of solution, equation (28) can be rewritten as:

$$X = X_a + jX_b \tag{29}$$

At a specific load angle (δ), the circuit of Fig. 4 will operate at unity power factor only when the imaginary part of the total impedance (Z_T) becomes zero. That is with the variation of the capacitor, unity power factor is obtained when X_e of equation (30) is zero.

$$Z_T = \mathrm{R}_{eq} + jX_{eq} \tag{30}$$

To illustrate the effect of the capacitance uniquely introduced through the auxiliary winding on the power factor of the machine, the imaginary part of the total machine impedance (X_{eq}) is plotted against the capacitance injected (C). The plot as shown in Fig. 14 is drawn for different load angles.

A closer look at Fig. 14 shows that for a given reluctance machine with the configuration discussed in this study, there is a wide range of load angle at which a high and good power factor is obtainable.

To verify the model and the results of the simulation, a practical experiment was conducted on a 3-Φ, 2kW, 4 – pole 50Hz machine with specifications as in the appendix. The machine was modified as described in Fig.1. The rotor structure is the conventional simple salient pole type. The measured power factor for both uncompensated and compensated with 20μF corroborate the predicted results as shown in Fig. 15. This figure further revealed that the compensated machine has a better power factor over all the operating range of this machine.

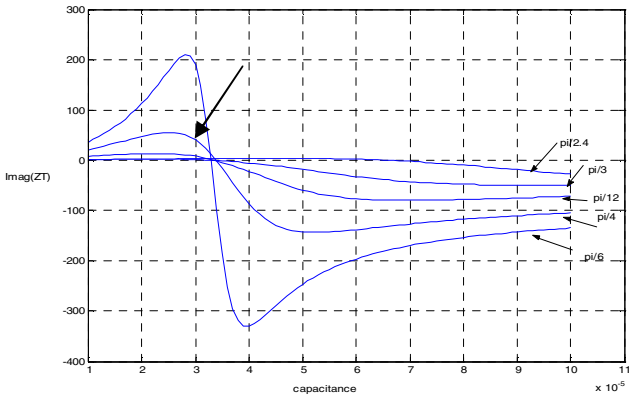

Fig. 14: Plot of the Imaginary part of Total Impedance against the Capacitance at different load angles.

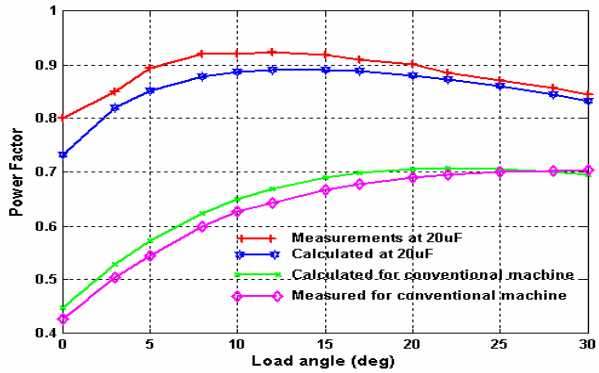

Fig. 15: Measured and calculated power factor of the machine (**with and without auxiliary winding connected to a capacitor**) as a function of the load angle

B. *Impact on Torque*

By the use of the magnetic field concepts, the average torque of the machine is derived from the rate of change of the stored energy in the magnetic circuit and can be written as:

$$T_{av} = p_r \frac{dE}{d\delta} \tag{31}$$

Consequently, the torque expression for the machine configuration discussed in this paper is obtained from equation (31) as:

$$T_{av1} = p_r \mu_o n r \pi l \left[\left(F_{ma}^2 \sin(2\delta) + F_{mx}^2 \sin(2\delta - 2\alpha_a) + F_{ma} F_{mx} \sin(2\delta + \alpha_a) \right) \right] \tag{32}$$

while the torque of the conventional synchronous reluctance machine is simply expressed as:

$$T_{avc} = p_r \mu_o n r \pi l F_{ma}^2 \sin(2\delta) \tag{33}$$

F_{ma} and F_{mx} respectively represent the peak value of the mmf due to the main and auxiliary winding; *n* is defined in terms of the airgap geometry of the machine, while *l* represents the magnetic length of the machine.

Comparatively, equations (32) and (33) show that for machine of the same dimensions, the machine discussed in this paper has a superior torque to the conventional synchronous reluctance machine. This is simply represented by equation (34).

$$T_{av1} - T_{avc} = p_r \mu_o n r \pi l \left[\left(F_{mx}^2 \sin(2\delta - 2\alpha_a) + F_{ma} F_{mx} \sin(2\delta + \alpha_a) \right) \right] \tag{34}$$

Fig. 16 shows the measured and predicted torque of the machine without compensation and with 20µF compensation. The relative torque performance improvement of the machine with the modified stator as expressed in equation (34) is easily observable in the plot of Fig. 16.

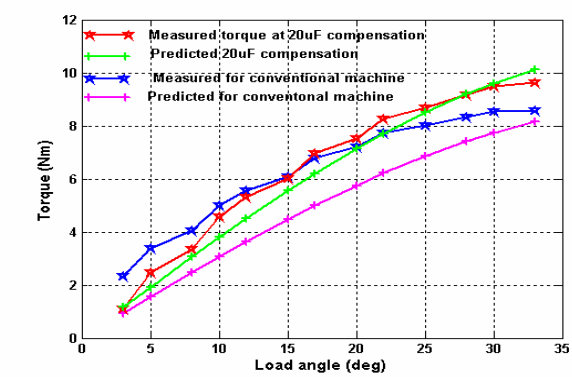

Fig. 16: Measured and predicted torque of the machine (**with and without auxiliary winding connected to a capacitor**) as a function of the load angle

Similarly, the variation of the measured torque of the machine configuration discussed here (T_{av1}) as a function of capacitance at different load angles is further illustrated in the contour plot of Figure 17. It is observed that the torque of this machine also varies with the capacitance at a fixed load angle. When the capacitance injected into the machine is varied from 5µF to 25µF an initial increase but of a small magnitude is noticed. This however will drop in magnitude as soon as the capacitance is further increased beyond certain capacitance value.

The size of capacitance that may be utilized as compensation in the auxiliary winding is greatly influenced by the conductor size of the winding. As for the experimental machine used in this work, the maximum capacitor that was utilized without endangering the auxiliary winding was 25µF.

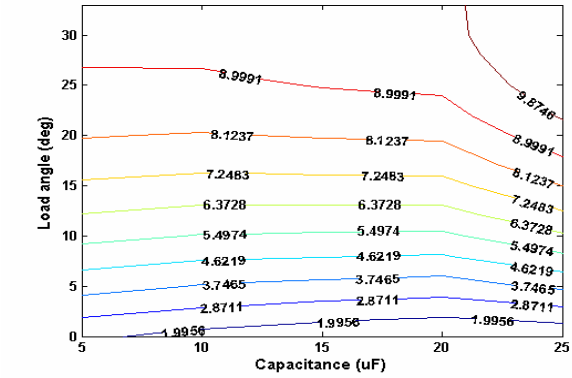

Fig.17: Contour Plots of the Torque (Tav1) as a function of Capacitance and delta

VI. CONCLUSION

In this paper, a synchronous reluctance machine that utilizes a balanced three phase auxiliary winding connected through a static switch to a capacitor for leading capacitance injection is explored for power factor improvement.

An equivalent circuit of the machine suitable for dynamic, steady state and transient analysis was developed and presented in this work. The steady state circuit was however used to investigate two switching topologies for leading reactive power injection. Similar results were obtained with these topologies, however, the bridge switch topology gave its result at a duty cycle of 60% and the capacitance requirement with the topology (BST) was also found to be smaller. Furthermore, the steady state characteristic of the presented scheme was studied and the possibility of unity power factor over a wide range of load angles was established. Experimental results were likewise used to corroborate the simulations. These improvements were obtained at reasonable main winding current. The promise of a relatively superior torque presented by this configuration was also experimentally justified. The presence of torque ripple associated with reluctance machine may still be obvious, and further study is to address this ripple in the torque using specially designed flux barrier rotor configuration.

REFERENCES

[1]. Agu, L.A., Anih, L.U.,Ojo J.O, Jimoh, A.A. 2005. *Novel Synchronous reluctance machines with Capacitance Injection*. LH Marthinusen Rotating Machine Conference, Pilansberg Conference centre, South Africa. pp.1-8.

[2]. Boldea I., Fu, X.Z., and Nasar, S.A. 1994.*Performance Evaluation Of Axially Laminated Anisotropic (ALA) Rotor Reluctance Synchronous Motors. IEEE Transactions on Industrial applications*, Vol. 30, No 4. pp. 977-985

[3]. Matsuo, T and Lipo, T.A, "*Rotor Design Optimisation of Synchronous Reluctance Machine*. IEEE Transaction on Energy Conversion, Vol. 9, No.2, pp 359-365.

[4]. Kamper, M.I .and Volschenk, A.F. 1994.*Effect of Rotor Dimensions and Cross Magnetisation on L_d and L_q Inductances Of Reluctance Synchronous Machine With Cageless Flux Barrier Rotor*. IEE Proceeding on Electrical Power Application, Vol. 141, and No 4. pp. 213-220.

[5]. Vagatti, A 1994. *"The Synchronous reluctance Machine Solution: a new Alternative In AC Drives"*. In proc. 20th int. Conference Industrial Electronics, control and Instrumentation, Vol. 1, Sept. pp1-13.

[6]. Toliyat ,H.A.,Shaleish P.W. and Lipo, T. (1998), 'Analysis *and simulation of Five phase Synchronous reluctance machines including Third Harmonic of Airgap MMF*'IEEE Transactions on Industry Applications, Vol.34, No. 2. pp 332-339.

[7]. Rakgati E.T and Kamper, M.I (2006) *Torque Performance of Optimally Designed Three and Five Phase Reluctance Synchronous Machines with Two rotor Structures*. SAIEE, Vol. 97(1) pp. 43-49.

[8]. Mujaldi, T.A. Lipo, and D.W. Novotny, '*Power Factor enhancement of Induction Machines by means of solid state excitation'*, Research report 86-3 of WEMPEC. 1986

[9]. Nicolae DV and Jimoh AA (2007) '*A Three Phase Induction Motor with power electronic controlled Single Phase Auxilliary Stator winding*. PECS 2007.

[10]. Suchi, M. Kansara, P. Holmes and W. Szabo, *Performance Enhancement of an Induction Motor by Secondary Impedance Control*, *IEEE Trans. On Energy Conversion*, Vol. 17, No. 2 June 2002

[11]. Bertz, R.E. et al. 1993. *Control of Synchronous Reluctance Machines*. IEEE Transactions on Industry Applications, Vol. 29, No. 6. pp. 1110-1122.

APPENDIX

Other parameters of the experimental machine include the following:

X_d=43.315Ω, X_q=12.601Ω, Main winding current = 8.8A, Main winding resistance= 4.766Ω.